Depletions of multi-MeV Electrons and Their Association to Minima in Phase Space Density

Alexander Yurievich Drozdov[1], Hayley J Allison[2], Yuri Y Shprits[3], Maria E. Usanova[4], Anthony A. Saikin[5], and Dedong Wang[6]

[1]University of California Los Angeles
[2]GFZ
[3]Helmholtz Centre Potsdam
[4]Laboratory for Atmospheric and Space Physics, University of Colorado Boulder
[5]University of California, Los Angeles
[6]GFZ German Research Center for Geosciences

November 23, 2022

Abstract

Fast-localized electron loss, resulting from interactions with electromagnetic ion cyclotron (EMIC) waves, can produce deepening minima in phase space density (PSD) radial profiles. Here, we perform a statistical analysis of local PSD minima to quantify how readily these are associated with radiation belt depletions. The statistics of PSD minima observed over a year are compared to the Versatile Electron Radiation Belts (VERB) simulations, both including and excluding EMIC waves. The observed minima distribution can only be achieved in the simulation including EMIC waves, indicating their importance in the dynamics of the radiation belts. By analyzing electron flux depletions in conjunction with the observed PSD minima, we show that, in the heart of the outer radiation belt (L*<5), up to 45% of multi-MeV electron depletions are associated with PSD minima, demonstrating that fast localized loss by interactions with EMIC waves are a common and crucial process for ultra-relativistic electron populations.

Hosted file

`essoar.10510085.1.docx` available at https://authorea.com/users/531399/articles/600911-depletions-of-multi-mev-electrons-and-their-association-to-minima-in-phase-space-density

A.Y. Drozdov[1*], H.J. Allison[2], Y.Y. Shprits[1, 2, 3], M. Usanova[4], A. Saikin[1], D. Wang[2]

[1] University of California Los Angeles, CA, USA

[2] GFZ German Centre for Geosciences, Potsdam, Germany

[3] Institute of Physics and Astronomy, University of Potsdam, Germany

[4] Laboratory for Atmospheric and Space Physics, University of Colorado Boulder, Boulder, Colorado, USA

Corresponding author: Alexander Drozdov (adrozdov@ucla.edu)

Key Points:

- PSD minima are commonly observed throughout a year of observations, indicating a major role of fast-localized losses of multi-MeV electrons.
- A modeled year reproduces the distribution of PSD minima over the same range of and K as observations only when EMIC waves are included.
- 28-45% of flux depletions below L*=5 ($\alpha_{eq} < 75$ °) are associated with PSD minima.

Abstract

Fast-localized electron loss, resulting from interactions with electromagnetic ion cyclotron (EMIC) waves, can produce deepening minima in phase space density (PSD) radial profiles. Here, we perform a statistical analysis of local PSD minima to quantify how readily these are associated with radiation belt depletions. The statistics of PSD minima observed over a year are compared to the Versatile Electron Radiation Belts (VERB) simulations, both including and excluding EMIC waves. The observed minima distribution can only be achieved in the simulation including EMIC waves, indicating their importance in the dynamics of the radiation belts. By analyzing electron flux depletions in conjunction with the observed PSD minima, we show that, in the heart of the outer radiation belt (L*<5), up to 45% of multi-MeV electron depletions are associated with PSD minima, demonstrating that fast localized loss by interactions with EMIC waves are a common and crucial process for ultra-relativistic electron populations.

Plain Language Summary

In this study, we explore the distribution of extremely high energy electrons that surround near-Earth space (from ~20.000 km up to ~35.000 km). Such electrons are trapped by the Earth's magnetic field, forming the radiation belt. There are several mechanisms of how such electrons can vanish. So-called phase space density profiles help us to distinguish between different causes of electron loss. Our statistical analysis of the minima in the phase space density profiles and additional comparison with the depletions of measured electron fluxes showed that a fast localized loss process is frequently acting in the heart of the radiation

belt. We associate this loss process with wave-particle interactions between electrons and space-originated electromagnetic ion cyclotron (EMIC) waves. This conclusion is confirmed by the modeling and demonstrates the importance of these waves in the dynamics of the radiation belts.

1 Introduction

Earth's outer radiation belt is a region of geomagnetically confined electrons and can contain particles with multi-MeV energies. Changes in the flux of the multi-MeV populations may be reversible (or adiabatic) or irreversible and can arise from a number of processes, including large-scale magnetic field fluctuations and wave-particle interactions with plasma waves. Analysis of phase space density (PSD) profiles (e.g., Green & Kivelson, 2004; Selesnick & Blake, 2000; Shprits et al., 2017; Turner et al., 2010; Tu et al., 2009) is a commonly used tool in radiation belt research to determine the relative contributions of population changes due to ULF activity (monotonic radial profiles) and local acceleration (growing peaks profiles) (Allison & Shprits, 2020; Baker et al., 2014; Chen et al., 2006; Iles et al., 2006; Olifer, Mann, Ozeke, Morley, et al., 2021; Reeves et al., 2013; Wu et al., 2020; Zhao et al., 2019). Shprits et al. (2017) also noted that local deepening minima occurring in PSD profiles can be indicative of fast localized loss processes, such as those resulting from resonant interactions with electromagnetic ion cyclotron (EMIC) waves.

EMIC waves are highly efficient at scattering multi-MeV electrons, and they can play a major role in the occurrence of rapid depletions in the heart of the radiation belts (Qin et al., 2019; Shprits et al., 2013, 2016, 2018; Ukhorskiy et al., 2010; Xiang et al., 2017). At the outer boundary of the electron radiation belt, electrons can also be rapidly depleted by the combination of magnetopause shadowing and outward radial diffusion (Elkington et al., 2003; Hudson et al., 2014; Turner et al., 2012; Tu et al., 2019; Ukhorskiy et al., 2009; Xiang et al., 2017). Turner et al. (2019) and Drozdov et al. (2019) showed that ~36% of storms result in a depletion of multi-MeV electrons, while for lower energies, this percentage was significantly lower, suggesting energy-dependent loss. Although studies have shown simultaneous observation of electron depletions below 1 MeV and EMIC wave activity (e.g., Capannolo, Li, Ma, Shen, et al., 2019), it is generally accepted that EMIC waves typically only resonate with higher energy electrons (Cao et al., 2017; Kersten et al., 2014; Mourenas et al., 2016; Zhang et al., 2016), with a minimum resonant energy commonly reported at ~2 MeV. Whether EMIC waves affect lower energy electrons remains an open question (e.g., Ripoll et al., 2020). Despite observed EMIC waves often being very radially localized (Usanova et al., 2008, 2016; Usanova & Mann, 2016) and transient (e.g., Blum et al., 2016, 2017; Wang et al., 2017), studies have explored their importance for local multi-MeV electron loss (e.g., Cervantes, Shprits, Aseev, Drozdov, et al., 2020; Drozdov et al., 2015, 2017; Xiang et al., 2018), however the overall impact of EMIC waves on radiation belts as a whole is a subject of ongoing research (e.g., Ripoll et al., 2020). The consequences of EMIC wave activity to the overall shape and dynamics of the radiation belts still remains

unknown.

To address the open questions raised above, we perform analysis of observed PSD profiles to identify when fast localized loss occurs and explore the effect of EMIC waves during these periods (e.g., Aseev et al., 2017; Blum et al., 2020; Capannolo, Li, Ma, Chen, et al., 2019; Kim et al., 2021; Ma et al., 2020; Xiang et al., 2017). In this study, PSD minima are automatically identified using one year of Van Allen Probes and GOES observations (1 October 2012 to 1 October 2013). Dropouts in the electron fluxes occurring in conjunction with PSD minima are analyzed. We consider whether the and K coverage, and therefore affected energy range, where PSD minima are typically observed is consistent with the current theory of EMIC wave-particle interactions. We perform a long-term simulation with the VERB model, both with and without EMIC waves included to determine their role. Minima in the modeled PSD profiles are identified, and the corresponding and K values are compared to those identified from observations over the same interval. How frequently the PSD minima corresponds to the multi-MeV electron flux depletion helps us to determine the significance of the fast-localized losses caused by EMIC waves in the dynamics of the radiation belts.

2 Data

For the electron flux and PSD analysis in this work, we use Van Allen Probes (Spence et al., 2013) and Geostationary Operational Environmental Satellite (GOES) observations. The Van Allen Probes are two identical spacecraft (A and B) orbiting at low inclination (less than 18°) between ~1.5 and ~6 Earth radii. GOES satellites operate at geostationary orbit. In this study, we use the GOES-15 satellite data from the Energetic Proton, Electron, and Alpha particle Detector (EPEAD) and the Magnetospheric Electron Detector (MAGED). Electron flux measurements from the Magnetic Electron Ion Spectrometer (MagEIS) (Blake et al., 2013) and the Relativistic Electron Proton Telescope (REPT) (Baker et al., 2013) are used from the Van Allen Probes. MagEIS measures electron energies from ~30 keV up to ~4 MeV, while REPT covers electron energies from ~2-10 MeV. EPEAD provides measurements in two integral flux channels, >800 keV and >2 MeV, while MAGED provides measurements of electron differential flux from ~30 keV up to ~600 keV.

We calculate PSD using a 5-minute averaged flux measurement. The adiabatic invariants, equatorial pitch angle, and L* were calculated using the TS05 magnetic field model (Tsyganenko & Sitnov, 2005) and the International Geomagnetic Reference Field (IGRF) internal magnetic field model.

3 Methodology

To perform the search for PSD minima, we use automatic identification of the local minima and maxima along the profile. Extrema were identified numerically. The results were validated against PSD minima that were found manually and published by Aseev et al. (2017). Note that Aseev et al. (2017) used fewer than 2 months of observations, 3 values of the first adiabatic invariant, , and one

value of the second adiabatic invariant, K. In our investigation, we extended the period of study (1 October 2012 to 1 October 2013) and the range of and K.

3.1 Data preparation

The Van Allen Probes and GOES data are processed to obtain PSD in the extended range of [1000, 5500] MeV/G (10 values, distributed linearly with the step of 500 MeV/G), and K [0.001, 1] $G^{1/2}R_E$ (10 values, with variable steps, e.g., K=0.001, 0.003, 0.007, 0.01...1 $G^{1/2}R_E$, see Figure 3). To obtain selected values of and K, we used interpolation and excluded points outside of the interpolation interval. We excluded the measurements that were lower than the background level determined similarly to Shprits et al. (2018, see Supplementary Information). Next, we binned PSD using median values on each orbital pass (separating inbound and outbound passes) of Van Allen Probes A and B on the L* grid with the step of 0.1, and extended the coverage at high L* using GOES observations.

The search for the PSD local minima depends only on the shape of the profile. Hence, we normalized PSD profiles according to equation (1):

$$\text{Norm. PSD} = \frac{\text{PSD}(L^*)}{\int_{L^*=3.5}^{L^*=5.5} \text{PSD}(L^*)dL^*} \quad (1)$$

The search of the local minima is performed in the range L* [3.5, 5.5]. The lower limit is in the proximity of the slot region, with many points being excluded due to the background noise, and the upper limit is defined as Van Allen Probes apogee (although GOES data are used to extend the profiles up to L*=5.5, when needed).

3.2 Determining the PSD minima search method

To determine local PSD minima, we performe a numerical search of local extrema. Figure 1a shows an example of a processed PSD profile. The robust identification of local minima that can be a result of localized loss requires a set of criteria, such as minimum's depth and width. To select the appropriate criteria, we calculate the ratio between the local minimum and the smallest adjacent local maximum. In Figure 1a, the smallest local maximum is located at L*=5.5, at the edge of the PSD profile. The minimum's depth criteria is determined by the ratio threshold (green line in Figure 1a). To exclude small variations that can result in a single point local minimum, and to define the minimum's width criteria, we require that at least 2 points must be below the ratio threshold. Hence, the narrowest localized PSD minimum that can be defined by this algorithm is 0.2 L* wide. In this study, as we focus on the effect of localized losses, we employ an additional criterion that PSD at the local minimum must be lower than for the previously available satellite pass. This criterion ensures that we only detect deepening minima.

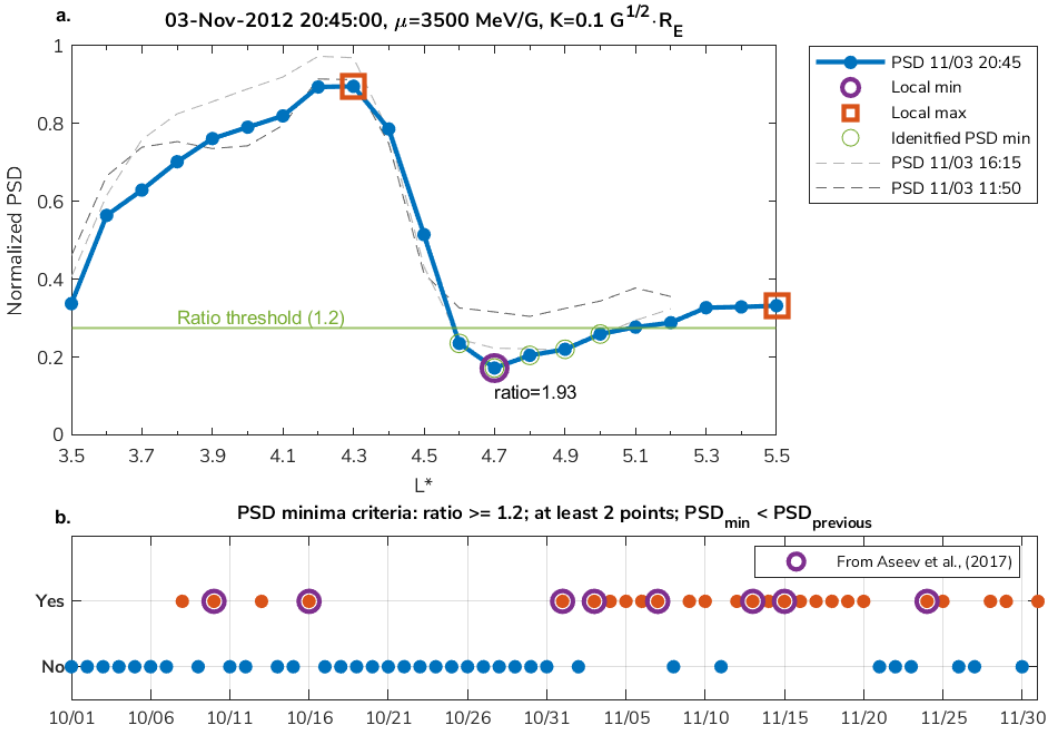

Figure 1. (a) Example of processed and normalized PSD profile (blue line). Purple and red markers are local minimum and maxima. Green line is the ratio threshold below which the PSD minima are identified (green markers). Gray profiles correspond to the PSD at the previously available pass, showing that the identified minimum is deepening. (b) Formation of the PSD minima between 9 October and 29 November 2012. Red points - automatically identified PSD minima (at least one per day). Blue points - days without formation of PSD minima. Purple circles - PSD minima identified by Aseev et al. (2017).

After establishing the identification criteria, we select the ratio threshold based on PSD minima that were identified in a previously published study. Aseev et al. (2017) consider the interval between 9 October and 29 November 2012, which showed multiple events of enhanced EMIC wave activity observed on the ground (Usanova et al., 2014). PSD profiles were analyzed for =2500, 3500, 4500 MeV/G at K=0.1 $G^{1/2}R_E$, and 8 events of the formation of the most pronounced minima in PSD profiles were found. Figure 1b shows the number of days when PSD minima are detected using our algorithm in comparison to the events manually found by Aseev et al. (2017). We successfully identify PSD minima when the ratio threshold is set to be >=1.2. Increasing the threshold led to the disappearance of the identified PSD minima among those from Aseev et al. (2017). Our algorithm identified more events than Aseev et al. (2017), because the authors focused on the first appearance of the pronounced PSD minima.

Several identified PSD minima are persistent and continued to decrease after the initial appearance. In Section 4, we compare the identified PSD minima events to associated electron flux depletions to identify the PSD minima driven by localized loss.

Using our algorithm, we perform the search of PSD minima for the one-year period. Following Aseev et al. (2017), the found minima are grouped daily. To confirm that the found PSD minima are a result of EMIC wave activity, we performe a numerical simulation using the Versatile Electron Radiation Belts (VERB) code.

3.3 The VERB code simulations

To perform long-term simulations (from 1 October 2012 to 1 October 2013) with and without EMIC waves, we use a similar setup as in Drozdov et al. (2017). The VERB code solves the Fokker-Planck equation using an approach of a single grid of modified adiabatic invariants (Subbotin & Shprits, 2012). The simulation includes Kp-driven hiss (Spasojevic et al., 2015) and chorus (Zhu et al., 2019) waves; constant lightning-generated whistler waves and very low frequency (VLF) waves from man-made transmitters (Subbotin et al., 2011). When enabled, EMIC waves are parameterized by solar wind dynamic pressure according to Drozdov et al. (2017). The plasmapause location is defined by Carpenter and Anderson (1992). We use the Kp-dependent Brautigam and Albert (2000) radial diffusion parameterization, which is consistent with our previous simulations, and provide optimal performance based on the comparative analysis among other parameterizations (see Drozdov et al., 2021). The initial and outer boundary (L*=5.5) conditions are defined based on Van Allen Probes measurements. Other boundary conditions and the size of the simulation domain are the same as in Drozdov et al. (2017). The simulation time step and the VERB code output is set to one hour.

3.4 Searching for multi-MeV electron flux depletion events

The analysis of multi-MeV electron flux depletions allows us to associate PSD minima with observed electron loss. In order to identify periods when the multi-MeV electrons show a net depletion, we bin the electron flux with a time step of 8 hours, and an L* step of 0.5. Then we perform a moving median analysis with a time window of 24 hours and calculate the difference between the logarithm of fluxes at the selected time and at the time mark, plus 24 hours. We defined a flux depletion event if the flux decreases by a factor of 3 within 24 hours according to equation (2):

$$\Delta \log_{10}(j) = \log_{10}(\overline{j_{t_0 \ldots t_0+24h}}) - \log_{10}(j_{t_0}) \leq \log_{10}(1/3) \quad (2)$$

The search of flux depletion events is performed within the following parameters. We select 9 energy channels using the REPT instrument (E [1.8, 9.9] MeV), 6 pitch angles ($\alpha_{\text{eq}} = 15^\circ,\ 30^\circ, 45^\circ, 60^\circ, 75^\circ, 85^\circ$), and 7 L* values (L* [3, 6], ΔL*=0.5). Note that we interpolate flux to obtain its values at fixed equatorial pitch angles.

Figures 2a and 2b show the example of 1.8 MeV and 4.2 MeV electron flux at $\alpha_{\mathrm{eq}} = 75$ °during the period of interest. Figures 2c and 2d show the line plots of the calculated difference of logarithm of flux, according to equation (2). The horizontal solid lines indicate the threshold of the electron flux depletion. When the line plots cross the threshold, the electron flux depletion event is identified (vertical dotted lines).

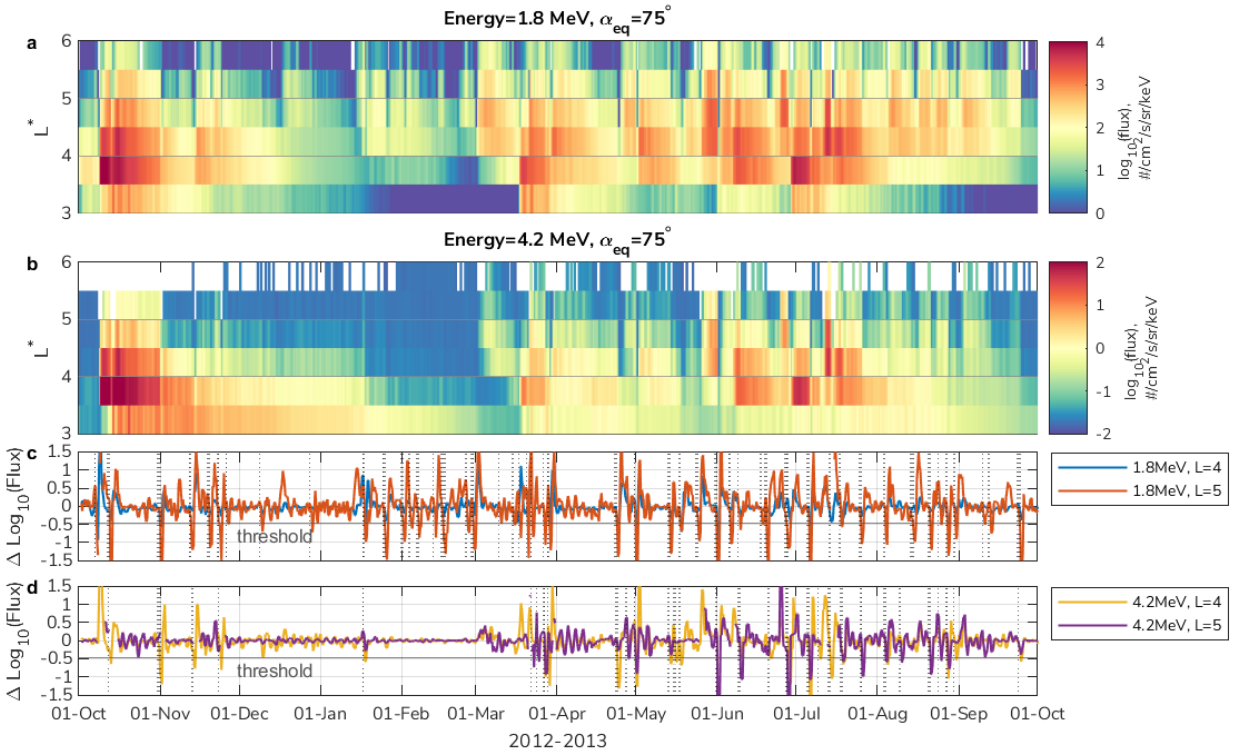

Figure 2. (a, b) Observed electron flux at $\alpha_{\mathrm{eq}} = 75^{\circ}$ at 1.8 and 4.2 MeV respectively. (c, d) $\Delta\log_{10}(j)$ constructed at L*=4 and L*=5, at 1.8 MeV and 4.2 MeV, respectively. Vertical dotted lines correspond to the found flux depletion events ($\Delta\log_{10}(j) \leq \log_{10}(1/3)$).

4 Results

4.1 Distribution of PSD minima

Figure 3a shows the distribution across and K, where deepening PSD minima are observed by Van Allen Probes and GOES. Each cell in the histogram corresponds to the number of days when PSD minima were observed. The statistics show that PSD minima are seen regularly, reaching hundreds of days or more in particular cells, over the year period. We see that for lower values of , PSD minima are seen most commonly at the highest values of K, and as increases, the most common K value for the deepening minima decreases. Figure 3b shows a

histogram in the same format as in Figure 3a, but with the distributions of PSD minima obtained from the VERB simulation with EMIC waves. The distribution across and K space of the modeled PSD depletions very closely resembles the distribution obtained from the observations, both in terms of the typical and K coverage and the trends seen. This agreement suggests that the parameterized model of the EMIC wave diffusion coefficients used in the simulation well covers the typical and K values, where the effects of EMIC waves are generally seen. A quantitative difference is, however, observed, which can be explained by the idealistic nature of the simulation results. The depletion of the PSD due to the EMIC waves strictly obeys diffusion process, while observations include small variations from orbit to orbit. This leads to some over-counting of the persistent minima that present after the electron flux depletion. The automatic algorithm periodically detects PSD at the minimum that is lower than on the previously available orbit, and therefore, counts it as an event, while the simulation results provide a stable and smooth PSD change and count only the individual occurrences of the flux depletion. Applying harder criteria to the algorithm to counter this effect led to the disappearance of the events found by Aseev et al. (2017). Nevertheless, the results of the simulation with EMIC waves are in good agreement with the dynamics of multi-MeV electrons fluxes, as shown by Drozdov et al. (2017).

The VERB simulation, which does not include EMIC waves, results in the absence of deepening PSD minima entirely (Figure 3d). Therefore, all PSD minima in the simulation with EMIC waves are a result of EMIC wave activity. Figure 3c shows pitch-angle diffusion coefficients due to EMIC waves (see Meredith et al., 2014) that are used in the simulation, and also presented in and K space. Once again, there is a close resemblance between the shape of the EMIC wave pitch-angle diffusion coefficient (Figure 3c) and where the deepening PSD minima were most readily observed in data (Figure 3a), suggesting that the quasi-linaer theory for the energy range over which EMIC waves are resonant is well supported by the occurrence distribution PSD minima observations. Additionally, the agreement between the observed and the modeledminima distributions shown in Figures 3a and b indicates that the observed PSD minima in Figure 3a are also likely the result of EMIC activity.

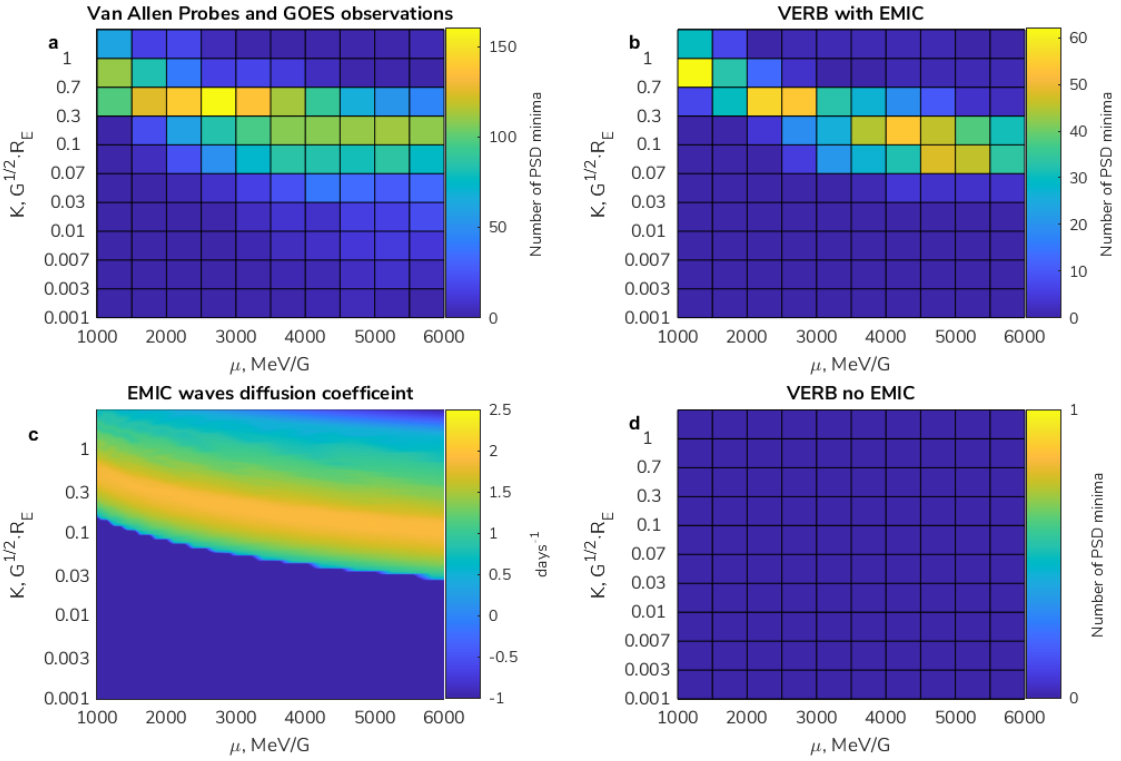

Figure 3. Distribution of the PSD minima in and K space. Each cell corresponds to the number of days when PSD minima were detected. The distribution is constructed based on: (a) Van Allen Probe and GOES observations, (b) VERB code simulation with EMIC waves, and (d) VERB code simulation without EMIC waves. (c) Example of EMIC wave pitch-angle diffusion coefficient in the same coordinates (and K) at L=4.

4.2 Conformity between PSD minima and electron flux depletions

The flux depletion events identified with the method in section 3.4 are now compared with the observed PSD minima. The first row in Figure 4 (a, b, c, and d) shows the statistics of all found flux depletions across different energies and L* for four values of equatorial pitch angle. No depletions are recorded at energies >7.7 MeV (deep purple color), simply because there is no electron flux above the background noise level. A noticeably large number of electron flux depletions occurred at L*>5, and such a distribution is similar at different pitch angles. This is consistent with the frequently occurring outward radial diffusion and magnetopause shadowing effect (e.g., Drozdov et al., 2019; Fei et al., 2006; Olifer, Mann, Ozeke, Claudepierre, et al., 2021; Xiang et al., 2017). The number of depletion events at L*>5 decreases with energy increase, because high-energy electrons less frequently occur in the radiation belts.

To compare the electron flux depletion events and PSD minima, we must com-

pare events in energy and pitch-angle space with PSD minima in the space of adiabatic invariants. To overcome this difficulty, we simplify our analysis, and, for each depletion event, we calculate and K using the dipole field. Then we search for PSD minima within ±12 hours at the nearest and K. The second row in Figure 4 (e, f, g, and h) shows the electron flux depletion events that are associated with PSD minima via this technique. There are significantly fewer depletion events at high equatorial pitch angle ($\alpha_{eq} = 75^{\circ}$) in comparison to the lower pitch angles ($\alpha_{eq} < 75^{\circ}$) when the associated PSD minima restriction is applied. This is consistent with diffusion by EMIC waves since, alone, they do not typically affect electrons with equatorial pitch angles near 90°, but are very effective at lower pitch angles (e.g., Glauert & Horne, 2005; Jordanova et al., 2008; Shprits et al., 2016; Usanova et al., 2014).

The last row in Figure 4 (i, j, k, and l) shows the percentage of the depletion events in panels a-b which are associated with local deepening minima in PSD (in comparison to all multi-MeV electron depletion events). We find that the percentage of depletion events associated with local deepening minima is dependent on the equatorial pitch angle. For the lowest equatorial pitch angle bin, we consider that, on average, 45% of the depletion events for L*<5 have an associated minimum in the PSD profiles, with many individual bins exceeding 60%, suggesting that EMIC wave scattering is partly responsible for the identified flux depletions at this pitch angle, despite the localized and transient nature of EMIC waves. At higher pitch angles, the percentage of associated events decreases, showing 28% for the 45° equatorial pitch angle bin; and 31% at 60°. Depletion events associated with PSD minima are infrequently observed at the high equatorial pitch angles (6% on average at L*<5 and $\alpha_{eq} = 75^{\circ}$, Figure 4l).

The percentages in Figure 4 also demonstrate that depletions with associated PSD minima are rarely observed at L*>5 (1%-16%, on average) and, as such, the flux depletions observed in this L* range are likely to be primarily due to magnetopause shadowing and associated effects. However, the observed small percentage of the depletions associated with PSD minima at $\alpha_{eq} = 75^{\circ}$can be a result of pitch-angle scattering by hiss and chorus waves, with assistance of EMIC waves at lower pitch angles (e.g., Drozdov et al., 2020).

The large percentage of depletion events associated with PSD minima indicates that, very often, the depletion of the multi-MeV electron radiation belts is linked to fast localized loss processes originating from EMIC wave activity, consistent with previous results (e.g., Cervantes, Shprits, Aseev, & Allison, 2020; Ross et al., 2021; Xiang et al., 2018).

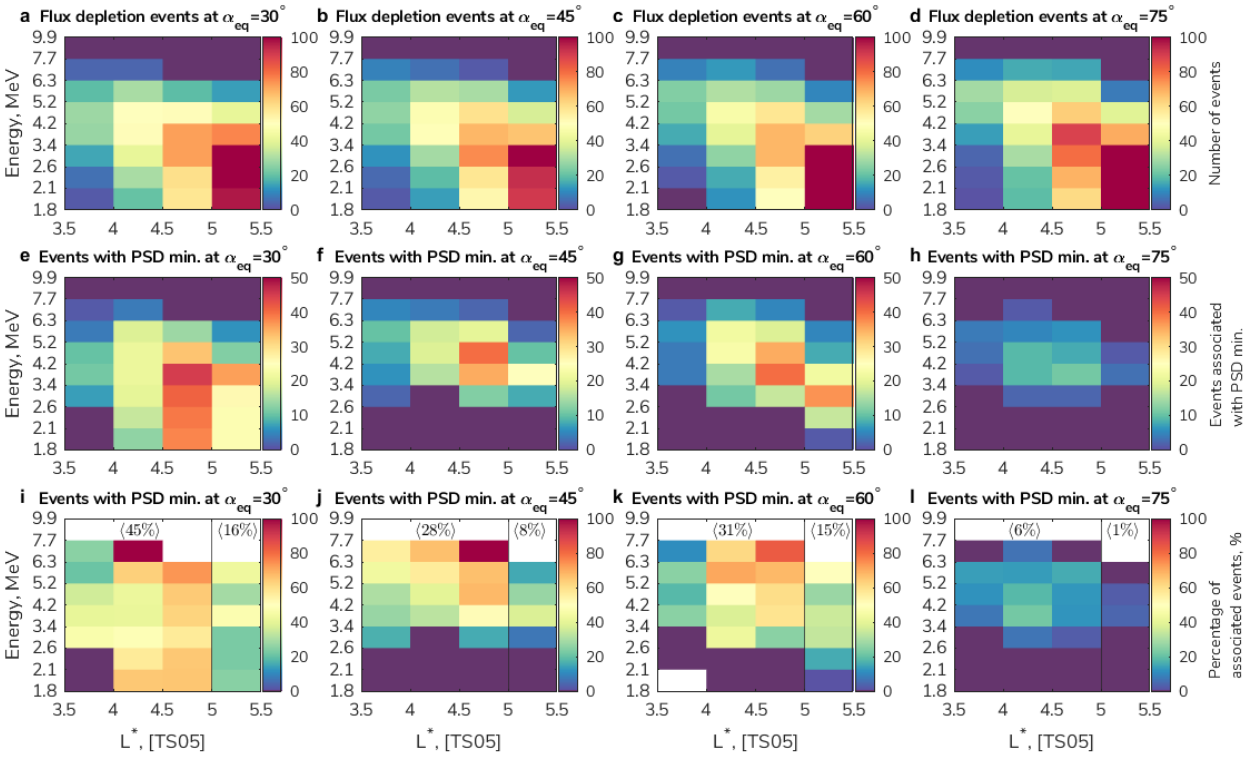

Figure 4. (a, b, c, d) Distribution of the electron flux depletion events in L* and energy space at different equatorial pitch angles (from left to right column: $\alpha_{eq} = 30°, 45°, 60°, 75°$, respectively). (e, f, g, h) Distribution of electron flux depletion events in conjunction with minima in PSD, at different pitch angles. (i, j, k, l) The percentage of the flux depletion events that are associated with PSD minima in comparison to all flux depletion events, at different pitch angles. Deep purple color corresponds to zero. White color corresponds to absence of the data in the bin due to division by zero (e.g., there are no electron flux depletion events). The numbers correspond to the averaging at L*>5 and L*<5 (black vertical line).

5 Conclusions

In this study, we performed a statistical analysis of the PSD minima and explored their relation to multi-MeV flux depletions. We find that the deepening minima in PSD, which can only be formed by a fast localized loss process, are commonly observed in the outer radiation belt at multi-MeV energies. The distribution of these observed PSD minima in and K space shows close agreement with both the EMIC wave diffusion coefficients as well as the distribution of PSD minima achieved in the VERB simulation with EMIC waves included. When EMIC wave activity was omitted from the simulation, deepening PSD minima were not identified. We therefore conclude that EMIC waves play a

significant role in the formation of PSD minima in the radiation belts and that the quasi-linear theory for the electron energy range affected by EMIC waves is well supported by the observed PSD minima occurrence distribution.

A high number of electron flux depletion events were identified at L*>5, likely a result of outward radial diffusion and magnetopause shadowing. Depletion events, which were associated PSD minima, were rarely observed at high equatorial pitch angle ($\alpha_{eq} = 75$), indicating the dominating role of other loss processes, aside from EMIC waves in this pitch angle range (despite possible EMIC wave scattering at lower pitch angle). For L*<5, simultaneous observations of multi-MeV electron flux depletions and PSD minima occurred often (from 28% to 45%, on average). The large percentage of electron flux depletion events (up to almost half) which were observed in conjunction with PSD minima profiles indicates the significant role of fast localized loss processes in the radiation belts.

Acknowledgments

This research is supported by NASA awards 80NSSC18K0663. HJA was supported by the Alexander von Humboldt society. This work used computational and storage services associated with the Hoffman2 Shared Cluster provided by the UCLA Institute for Digital Research and Education's Research Technology Group. The authors acknowledge the developers of the International Radiation Belt Environment Modeling (IRBEM) library. The authors would like to thank Sharon Uy for proofreading this manuscript.

Open Research

We thank the Van Allen Probe ECT team for providing the data (https://rbsp-ect.newmexicoconsortium.org/). The GOES measurements are available at the NOAA NGDC website (https://ngdc.noaa.gov/stp/satellite/goes/dataaccess.html). The authors used geomagnetic indices provided by OMNIWeb (https://omniweb.gsfc.nasa.gov/). The data to reproduce the figures are available at UCLA dataverse repository (https://doi.org/10.25346/S6/B05T1T).

References

Allison, H. J., & Shprits, Y. Y. (2020). Local heating of radiation belt electrons to ultra-relativistic energies. *Nature Communications*, *11*(1), 4533. https://doi.org/10.1038/s41467-020-18053-z

Aseev, N. A., Shprits, Y. Y., Drozdov, A. Y., Kellerman, A. C., Usanova, M. E., Wang, D., & Zhelavskaya, I. S. (2017). Signatures of Ultrarelativistic Electron Loss in the Heart of the Outer Radiation Belt Measured by Van Allen Probes. *Journal of Geophysical Research, [Space Physics]*, *122*(10), 2017JA024485. https://doi.org/10.1002/2017JA024485

Baker, D. N., Kanekal, S. G., Hoxie, V. C., Batiste, S., Bolton, M., Li, X., et al. (2013). The Relativistic Electron-Proton Telescope (REPT) Instrument on Board the Radiation Belt Storm Probes (RBSP) Spacecraft: Characterization

of Earth's Radiation Belt High-Energy Particle Populations. *Space Science Reviews*, *179*(1-4), 337–381. https://doi.org/10.1007/s11214-012-9950-9

Baker, D. N., Jaynes, A. N., Li, X., Henderson, M. G., Kanekal, S. G., Reeves, G. D., et al. (2014). Gradual diffusion and punctuated phase space density enhancements of highly relativistic electrons: Van Allen Probes observations. *Geophysical Research Letters*, *41*(5), 1351–1358. https://doi.org/10.1002/2013GL058942

Blake, J. B., Carranza, P. A., Claudepierre, S. G., Clemmons, J. H., Crain, W. R., Jr., Dotan, Y., et al. (2013). The Magnetic Electron Ion Spectrometer (MagEIS) Instruments Aboard the Radiation Belt Storm Probes (RBSP) Spacecraft. *Space Science Reviews*, *179*(1-4), 383–421. https://doi.org/10.1007/s11214-013-9991-8

Blum, L. W., Agapitov, O., Bonnell, J. W., Kletzing, C., & Wygant, J. (2016). EMIC wave spatial and coherence scales as determined from multi-point Van Allen Probe measurements. *Geophysical Research Letters*, *43*(10), 2016GL068799. https://doi.org/10.1002/2016GL068799

Blum, L. W., Bonnell, J. W., Agapitov, O., Paulson, K., & Kletzing, C. (2017). EMIC wave scale size in the inner magnetosphere: Observations from the dual Van Allen Probes. *Geophysical Research Letters*, *44*(3), 2016GL072316. https://doi.org/10.1002/2016GL072316

Blum, L. W., Remya, B., Denton, M. H., & Schiller, Q. (2020). Persistent EMIC wave activity across the nightside inner magnetosphere. *Geophysical Research Letters*, *47*(6). https://doi.org/10.1029/2020gl087009

Brautigam, D. H., & Albert, J. M. (2000). Radial diffusion analysis of outer radiation belt electrons during the October 9, 1990, magnetic storm. *Journal of Geophysical Research*, *105*(A1), 291–309. https://doi.org/10.1029/1999ja900344

Cao, X., Shprits, Y. Y., Ni, B., & Zhelavskaya, I. S. (2017). Scattering of Ultra-relativistic Electrons in the Van Allen Radiation Belts Accounting for Hot Plasma Effects. *Scientific Reports*, *7*(1), 17719. https://doi.org/10.1038/s41598-017-17739-7

Capannolo, L., Li, W., Ma, Q., Chen, L., Shen, X.-C., Spence, H. E., et al. (2019). Direct observation of subrelativistic electron precipitation potentially driven by EMIC waves. *Geophysical Research Letters*, *46*(22), 12711–12721. https://doi.org/10.1029/2019gl084202

Capannolo, L., Li, W., Ma, Q., Shen, X.-C., Zhang, X.-J., Redmon, R. J., et al. (2019). Energetic electron precipitation: Multievent analysis of its spatial extent during EMIC wave activity. *Journal of Geophysical Research, [Space Physics]*, *124*(4), 2466–2483. https://doi.org/10.1029/2018ja026291

Carpenter, D. L., & Anderson, R. R. (1992). An ISEE/whistler model of equatorial electron density in the magnetosphere. *Journal of Geophysical Research, [Space Physics]*, *97*(A2), 1097–1108. https://doi.org/10.1029/91JA01548

Cervantes, S., Shprits, Y. Y., Aseev, N. A., Drozdov, A. Y., Castillo, A., & Stolle, C. (2020). Identifying radiation belt electron source and loss processes by assimilating spacecraft data in a three-dimensional diffusion model. *Journal of Geophysical Research, [Space Physics]*, *125*(1). https://doi.org/10.1029/2019ja027514

Cervantes, S., Shprits, Y. Y., Aseev, N. A., & Allison, H. J. (2020). Quantifying the effects of EMIC wave scattering and magnetopause shadowing in the outer electron radiation belt by means of data assimilation. *Journal of Geophysical Research, [Space Physics]*, *125*(8). https://doi.org/10.1029/2020ja028208

Chen, Y., Friedel, R. H. W., & Reeves, G. D. (2006). Phase space density distributions of energetic electrons in the outer radiation belt during two Geospace Environment Modeling Inner Magnetosphere/Storms selected storms. *Journal of Geophysical Research*, *111*(A11). https://doi.org/10.1029/2006JA011703

Drozdov, A. Y., Shprits, Y. Y., Orlova, K. G., Kellerman, A. C., Subbotin, D. A., Baker, D. N., et al. (2015). Energetic, relativistic, and ultrarelativistic electrons: Comparison of long-term VERB code simulations with Van Allen Probes measurements. *Journal of Geophysical Research, [Space Physics]*, *120*(5), 3574–3587. https://doi.org/10.1002/2014JA020637

Drozdov, A. Y., Shprits, Y. Y., Usanova, M. E., Aseev, N. A., Kellerman, A. C., & Zhu, H. (2017). EMIC wave parameterization in the long-term VERB code simulation. *Journal of Geophysical Research, [Space Physics]*, *122*(8), 2017JA024389. https://doi.org/10.1002/2017JA024389

Drozdov, A. Y., Aseev, N., Effenberger, F., Turner, D. L., Saikin, A., & Shprits, Y. Y. (2019). Storm Time Depletions of Multi-MeV Radiation Belt Electrons Observed at Different Pitch Angles. *Journal of Geophysical Research, [Space Physics]*, *108*, 1249. https://doi.org/10.1029/2019JA027332

Drozdov, A. Y., Usanova, M. E., Hudson, M. K., Allison, H. J., & Shprits, Y. Y. (2020). The Role of Hiss, Chorus, and EMIC Waves in the Modeling of the Dynamics of the Multi-MeV Radiation Belt Electrons. *Journal of Geophysical Research, [Space Physics]*, *125*(9), 2628. https://doi.org/10.1029/2020JA028282

Drozdov, A. Y., Allison, H. J., Shprits, Y. Y., Elkington, S. R., & Aseev, N. A. (2021). A comparison of radial diffusion coefficients in 1-D and 3-D long-term radiation belt simulations. *Journal of Geophysical Research, [Space Physics]*, *126*(8). https://doi.org/10.1029/2020ja028707

Elkington, S. R., Hudson, M. K., & Chan, A. A. (2003). Resonant acceleration and diffusion of outer zone electrons in an asymmetric geomagnetic field. *Journal of Geophysical Research, [Space Physics]*, *108*(A3). https://doi.org/10.1029/2001JA009202

Fei, Y., Chan, A. A., Elkington, S. R., & Wiltberger, M. J. (2006). Radial diffusion and MHD particle simulations of relativistic electron transport by ULF

waves in the September 1998 storm. *Journal of Geophysical Research*, *111*(A12), A12209. https://doi.org/10.1029/2005JA011211

Glauert, S. A., & Horne, R. B. (2005). Calculation of pitch angle and energy diffusion coefficients with the PADIE code. *Journal of Geophysical Research, [Space Physics]*, *110*(A4). https://doi.org/10.1029/2004JA010851

Green, J. C., & Kivelson, M. G. (2004). Relativistic electrons in the outer radiation belt: Differentiating between acceleration mechanisms. *Journal of Geophysical Research*, *109*(A3), A03213. https://doi.org/10.1029/2003JA010153

Hudson, M. K., Baker, D. N., Goldstein, J., Kress, B. T., Paral, J., Toffoletto, F. R., & Wiltberger, M. (2014). Simulated magnetopause losses and Van Allen Probe flux dropouts. *Geophysical Research Letters*, *41*(4), 1113–1118. https://doi.org/10.1002/2014GL059222

Iles, R. H. A., Meredith, N. P., Fazakerley, A. N., & Horne, R. B. (2006). Phase space density analysis of the outer radiation belt energetic electron dynamics. *Journal of Geophysical Research*, *111*(A3), A03204. https://doi.org/10.1029/2005JA011206

Jordanova, V. K., Albert, J., & Miyoshi, Y. (2008). Relativistic electron precipitation by EMIC waves from self-consistent global simulations. *Journal of Geophysical Research*, *113*(A3), A00A10. https://doi.org/10.1029/2008JA013239

Kersten, T., Horne, R. B., Glauert, S. A., Meredith, N. P., Fraser, B. J., & Grew, R. S. (2014). Electron losses from the radiation belts caused by EMIC waves. *Journal of Geophysical Research, [Space Physics]*, *119*(11), 8820–8837. https://doi.org/10.1002/2014JA020366

Kim, H., Schiller, Q., Engebretson, M. J., Noh, S., Kuzichev, I., Lanzerotti, L. J., et al. (2021). Observations of particle loss due to injection-associated electromagnetic ion cyclotron waves. *Journal of Geophysical Research, [Space Physics]*, *126*(2). https://doi.org/10.1029/2020ja028503

Ma, X., Department of Space Physics, School of Electronic Information, Wuhan University, Wuhan 430072, China, Xiang, Z., Ni, B., Fu, S., Cao, X., et al. (2020). On the loss mechanisms of radiation belt electron dropouts during the 12 September 2014 geomagnetic storm. *Earth and Planetary Physics*, *4*(6), 1–13. https://doi.org/10.26464/epp2020060

Meredith, N. P., Horne, R. B., Kersten, T., Fraser, B. J., & Grew, R. S. (2014). Global morphology and spectral properties of EMIC waves derived from CRRES observations. *Journal of Geophysical Research, [Space Physics]*, *119*(7), 5328–5342. https://doi.org/10.1002/2014JA020064

Mourenas, D., Artemyev, A. V., Ma, Q., Agapitov, O. V., & Li, W. (2016). Fast dropouts of multi-MeV electrons due to combined effects of EMIC and whistler mode waves. *Geophysical Research Letters*, *43*(9), 4155–4163. https://doi.org/10.1002/2016GL068921

Olifer, L., Mann, I. R., Ozeke, L. G., Morley, S. K., & Louis, H. L. (2021). On the formation of phantom electron phase space density peaks in single spacecraft radiation belt data. *Geophysical Research Letters*, *48*(11). https://doi.org/10.1029/2020gl092351

Olifer, L., Mann, I. R., Ozeke, L. G., Claudepierre, S. G., Baker, D. N., & Spence, H. E. (2021). On the similarity and repeatability of fast radiation belt loss: Role of the last closed drift shell. *Journal of Geophysical Research, [Space Physics]*. https://doi.org/10.1029/2021ja029957

Qin, M., Hudson, M., Li, Z., Millan, R., Shen, X., Shprits, Y., et al. (2019). Investigating Loss of Relativistic Electrons Associated With EMIC Waves at Low L Values on 22 June 2015. *Journal of Geophysical Research, [Space Physics]*, *124*, 561. https://doi.org/10.1029/2018JA025726

Reeves, G. D., Spence, H. E., Henderson, M. G., Morley, S. K., Friedel, R. H. W., Funsten, H. O., et al. (2013). Electron acceleration in the heart of the Van Allen radiation belts. *Science*, *341*(6149), 991–994. https://doi.org/10.1126/science.1237743

Ripoll, J.-F., Claudepierre, S. G., Ukhorskiy, A. Y., Colpitts, C., Li, X., Fennell, J. F., & Crabtree, C. (2020). Particle dynamics in the earth's radiation belts: Review of current research and open questions. *Journal of Geophysical Research, [Space Physics]*, *125*(5). https://doi.org/10.1029/2019ja026735

Ross, J. P. J., Glauert, S. A., Horne, R. B., Watt, C. E. J., & Meredith, N. P. (2021). On the variability of EMIC waves and the consequences for the relativistic electron radiation belt population. *Journal of Geophysical Research, [Space Physics]*, *126*(12). https://doi.org/10.1029/2021ja029754

Selesnick, R. S., & Blake, J. B. (2000). On the source location of radiation belt relativistic electrons. *Journal of Geophysical Research*, *105*(A2), 2607. https://doi.org/10.1029/1999JA900445

Shprits, Y. Y., Subbotin, D., Drozdov, A., Usanova, M. E., Kellerman, A., Orlova, K., et al. (2013). Unusual stable trapping of the ultrarelativistic electrons in the Van Allen radiation belts. *Nature Physics*, *9*(11), 699–703. https://doi.org/10.1038/nphys2760

Shprits, Y. Y., Drozdov, A. Y., Spasojevic, M., Kellerman, A. C., Usanova, M. E., Engebretson, M. J., et al. (2016). Wave-induced loss of ultra-relativistic electrons in the Van Allen radiation belts. *Nature Communications*, *7*, 12883. https://doi.org/10.1038/ncomms12883

Shprits, Y. Y., Kellerman, A., Aseev, N., Drozdov, A. Y., & Michaelis, I. (2017). Multi-MeV electron loss in the heart of the radiation belts. *Geophysical Research Letters*, *44*(3), 2016GL072258. https://doi.org/10.1002/2016GL072258

Shprits, Y. Y., Horne, R. B., Kellerman, A. C., & Drozdov, A. Y. (2018). The dynamics of Van Allen belts revisited. *Nature Physics*, *14*, 102. https://doi.org/10.1038/nphys4350

Spasojevic, M., Shprits, Y. Y., & Orlova, K. (2015). Global empirical models of plasmaspheric hiss using Van Allen Probes. *Journal of Geophysical Research, [Space Physics]*, *120*(12), 2015JA021803. https://doi.org/10.1002/2015JA021803

Spence, H. E., Reeves, G. D., Baker, D. N., Blake, J. B., Bolton, M., Bourdarie, S., et al. (2013). Science Goals and Overview of the Radiation Belt Storm Probes (RBSP) Energetic Particle, Composition, and Thermal Plasma (ECT) Suite on NASA's Van Allen Probes Mission. *Space Science Reviews*, *179*(1), 311–336. https://doi.org/10.1007/s11214-013-0007-5

Subbotin, D. A., & Shprits, Y. Y. (2012). Three-dimensional radiation belt simulations in terms of adiabatic invariants using a single numerical grid. *Journal of Geophysical Research*, *117*(A5), A05205. https://doi.org/10.1029/2011JA017467

Subbotin, D. A., Shprits, Y. Y., & Ni, B. (2011). Long-term radiation belt simulation with the VERB 3-D code: Comparison with CRRES observations. *Journal of Geophysical Research, [Space Physics]*, *116*(A12), A12210. https://doi.org/10.1029/2011JA017019

Tsyganenko, N. A., & Sitnov, M. I. (2005). Modeling the dynamics of the inner magnetosphere during strong geomagnetic storms. *Journal of Geophysical Research*, *110*(A3), 7737. https://doi.org/10.1029/2004JA010798

Turner, D. L., Li, X., Reeves, G. D., & Singer, H. J. (2010). On phase space density radial gradients of Earth's outer-belt electrons prior to sudden solar wind pressure enhancements: Results from distinctive events and a superposed epoch analysis: PSD GRADIENTS OF OUTER-BELT ELECTRONS. *Journal of Geophysical Research*, *115*(A1). https://doi.org/10.1029/2009JA014423

Turner, D. L., Shprits, Y., Hartinger, M., & Angelopoulos, V. (2012). Explaining sudden losses of outer radiation belt electrons during geomagnetic storms. *Nature Physics*, *8*(3), 208–212. https://doi.org/10.1038/nphys2185

Turner, D. L., Kilpua, E. K. J., Hietala, H., Claudepierre, S. G., O'Brien, T. P., Fennell, J. F., et al. (2019). The response of Earth's electron radiation belts to geomagnetic storms: Statistics from the Van Allen Probes era including effects from different storm drivers. *Journal of Geophysical Research, [Space Physics]*. https://doi.org/10.1029/2018JA026066

Tu, W., Li, X., Chen, Y., Reeves, G. D., & Temerin, M. (2009). Storm-dependent radiation belt electron dynamics. *Journal of Geophysical Research*, *114*(A2). https://doi.org/10.1029/2008JA013480

Tu, W., Xiang, Z., & Morley, S. K. (2019). Modeling the magnetopause shadowing loss during the June 2015 dropout event. *Geophysical Research Letters*, *46*(16), 9388–9396. https://doi.org/10.1029/2019gl084419

Ukhorskiy, A. Y., Sitnov, M. I., Takahashi, K., & Anderson, B. J. (2009). Radial transport of radiation belt electrons due to stormtime Pc5 waves. *Annales Geophysicae*, *27*(5), 2173–2181. https://doi.org/10.5194/angeo-27-2173-2009

Ukhorskiy, A. Y., Shprits, Y. Y., Anderson, B. J., Takahashi, K., & Thorne, R. M. (2010). Rapid scattering of radiation belt electrons by storm-time EMIC waves: RADIATION BELT LOSS DUE TO EMIC WAVES. *Geophysical Research Letters*, *37*(9). https://doi.org/10.1029/2010GL042906

Usanova, M. E., & Mann, I. R. (2016). Understanding the Role of EMIC Waves in Radiation Belt and Ring Current Dynamics: Recent Advances. In *Waves, Particles, and Storms in Geospace: A Complex Interplay* (pp. 244–276). Oxford: Oxford University Press. https://doi.org/10.1093/acprof:oso/9780198705246.003.0011

Usanova, M. E., Mann, I. R., Rae, I. J., Kale, Z. C., Angelopoulos, V., Bonnell, J. W., et al. (2008). Multipoint observations of magnetospheric compression-related EMIC Pc1 waves by THEMIS and CARISMA. *Geophysical Research Letters*, *35*(17). https://doi.org/10.1029/2008gl034458

Usanova, M. E., Drozdov, A., Orlova, K., Mann, I. R., Shprits, Y., Robertson, M. T., et al. (2014). Effect of EMIC waves on relativistic and ultrarelativistic electron populations: Ground-based and Van Allen Probes observations. *Geophysical Research Letters*, *41*(5), 1375–1381. https://doi.org/10.1002/2013GL059024

Usanova, M. E., Mann, I. R., & Darrouzet, F. (2016). EMIC waves in the inner magnetosphere. In *Low-Frequency Waves in Space Plasmas* (pp. 65–78). Hoboken, NJ: John Wiley & Sons, Inc. https://doi.org/10.1002/9781119055006.ch5

Wang, X. Y., Huang, S. Y., Allen, R. C., Fu, H. S., Deng, X. H., Zhou, M., et al. (2017). The occurrence and wave properties of EMIC waves observed by the Magnetospheric Multiscale (MMS) mission. *Journal of Geophysical Research, [Space Physics]*, *122*(8), 8228–8240. https://doi.org/10.1002/2017ja024237

Wu, H., Chen, T., Kalegaev, V. V., Panasyuk, M. I., Vlasova, N. A., Duan, S., et al. (2020). Long-term dropout of relativistic electrons in the outer radiation belt during two sequential geomagnetic storms. *Journal of Geophysical Research, [Space Physics]*, *125*(10). https://doi.org/10.1029/2020ja028098

Xiang, Z., Tu, W., Li, X., Ni, B., Morley, S. K., & Baker, D. N. (2017). Understanding the Mechanisms of Radiation Belt Dropouts Observed by Van Allen Probes. *Journal of Geophysical Research, [Space Physics]*, *122*(10), 9858–9879. https://doi.org/10.1002/2017JA024487

Xiang, Z., Tu, W., Ni, B., Henderson, M. G., & Cao, X. (2018). A Statistical Survey of Radiation Belt Dropouts Observed by Van Allen Probes. *Geophysical Research Letters*, *45*(16), 8035–8043. https://doi.org/10.1029/2018GL078907

Zhang, X.-J., Li, W., Ma, Q., Thorne, R. M., Angelopoulos, V., Bortnik, J., et al. (2016). Direct evidence for EMIC wave scattering of relativistic electrons in space: EMIC-Driven Electron Losses in Space. *Journal of Geophysical Research, [Space Physics]*, *121*(7), 6620–6631. https://doi.org/10.1002/2016JA022521

Zhao, H., Baker, D. N., Li, X., Malaspina, D. M., Jaynes, A. N., & Kanekal, S. G. (2019). On the acceleration mechanism of ultrarelativistic electrons in the center

of the outer radiation belt: A statistical study. *Journal of Geophysical Research, [Space Physics]*, *124*(11), 8590–8599. https://doi.org/10.1029/2019ja027111

Zhu, H., Shprits, Y. Y., Spasojevic, M., & Drozdov, A. Y. (2019). New hiss and chorus waves diffusion coefficient parameterizations from the Van Allen Probes and their effect on long-term relativistic electron radiation-belt VERB simulations. *Journal of Atmospheric and Solar-Terrestrial Physics*, *193*, 105090. https://doi.org/10.1016/j.jastp.2019.105090